

# A Multi-Wavelength, Multi-Epoch Study of the Soft X-Ray Transient Prototype, V616 Mon (A0620-00)<sup>1</sup>

Dawn M. Gelino,<sup>2</sup> Thomas E. Harrison<sup>3</sup>

dleeber@nmsu.edu, tharriso@nmsu.edu

*Department of Astronomy, New Mexico State University, Las Cruces, NM 88003*

Jerome A. Orosz

J.A.Orosz@astro.uu.nl

*Astronomical Institute, Utrecht University, PO Box 80000, NL-3508 TA Utrecht, The Netherlands*

## ABSTRACT

We have obtained optical and infrared photometry of the soft x-ray transient prototype V616 Mon (A0620-00). From this photometry, we find a spectral type of K4 for the secondary star in the system, which is consistent with spectroscopic observations. We present  $J$ -,  $H$ -, and  $K$ - band light curves modeled with WD98 and ELC. Combining detailed, independently run models for ellipsoidal variations due to a spotted, non-spherical secondary star, and the observed ultraviolet to infrared spectral energy distribution of the system, we show that the most likely value for the orbital inclination is  $40.75 \pm 3^\circ$ . This inclination angle implies a primary black hole mass of  $11.0 \pm 1.9 M_\odot$ .

*Subject headings:* binaries: close – stars: black holes – stars: individual (V616 Mon) – stars: low mass – stars: variables: other

## 1. Introduction

Soft X-Ray Transients (SXTs) are a family of low mass X-ray binaries that display infrequent, but large and abrupt X-ray and optical outbursts that are believed to be the result of a sudden,

---

<sup>1</sup>This work was partly based on observations obtained with the Apache Point Observatory 3.5-meter telescope, which is owned and operated by the Astrophysical Research Consortium.

<sup>2</sup>Visiting Astronomer, Kitt Peak National Observatory, National Optical Astronomy Observatory, which is operated by the Association of Universities for Research in Astronomy, Inc. (AURA) under cooperative agreement with the National Science Foundation.

<sup>3</sup>Visiting Astronomer, Cerro Tololo Inter-American Observatory, National Optical Astronomy Observatory, which is operated by the Association of Universities for Research in Astronomy, Inc. (AURA) under cooperative agreement with the National Science Foundation.

dramatic increase in the mass accretion rate onto the compact object. In most cases the compact object is a black hole and the companion star is a low-mass K- or M-type dwarf (see Charles 2001 for a recent review). During their long periods of quiescence, SXTs are very faint at X-ray and optical wavelengths, however, in this state, the secondary stars can dominate the system luminosity and allow us to derive the SXT parameters.

The SXT prototype, V616 Mon (=A0620-00) ( $\alpha_{2000} = 06^{\text{h}}22^{\text{m}}44^{\text{s}}.4$ ,  $\delta_{2000} = -00^{\circ}20'45''$ ) was discovered by the Ariel-5 satellite on 1975 August 3 (Elvis et al. 1975), while the optical counterpart to the X-ray source was identified by Boley & Wolfson (1975). By studying the optical spectrum of the system, Oke (1977) found that one component of the light came from a K5 - K7 dwarf, and another from a suspected accretion disk. Since V616 Mon has faded from outburst, it has been studied by McClintock & Remillard (1986), Haswell et al. (1993, hereafter HRHSA), Marsh, Robinson, & Wood (1994, hereafter MRW), Shahbaz, Naylor, & Charles (1994, hereafter SNC), Froning & Robinson (2001, hereafter FR), and references therein. These authors have found an orbital period of 7.75 hours, a secondary star spectral type of K3V - K4V, and a secondary star radial velocity semi-amplitude of  $433 \pm 3 \text{ km s}^{-1}$ . V616 Mon therefore has an implied optical mass function, which is the minimum mass of the compact primary object, of  $2.72 \pm 0.06 M_{\odot}$  (MRW).

McClintock & Remillard (2000) report the X-ray luminosity of V616 Mon in quiescence is  $L_X \approx 6 \times 10^{30} \text{ erg s}^{-1}$ , and exhibits a very low accretion rate ( $\dot{M}_d \sim 10^{-10} M_{\odot} \text{ yr}^{-1}$ ). Therefore, the current quiescent light curves should be primarily governed by the light from the secondary star. Since the secondary star fills its Roche lobe, the amount of surface area seen by an observer on Earth changes as the star orbits the compact object. This changing line-of-sight surface area corresponds to a changing apparent brightness, giving rise to the so-called ellipsoidal variations. The amplitude of these variations is determined by the orbital inclination angle and mass ratio of the system. By combining the orbital inclination angle with the observed mass function, the SXT system parameters can be determined. In an effort to quell the debate over the inclination angle of the SXT prototype, we have obtained new optical and multi-epoch infrared photometry of V616 Mon. We have used two different light curve modeling programs to interpret the infrared ellipsoidal variations observed over a 22.5 month interval. We have previously used a similar technique to model GU Mus (Gelino, Harrison, & McNamara 2001, hereafter Paper 1), an SXT that closely resembles V616 Mon.

Most previous attempts to derive the orbital parameters for V616 Mon have used optical data. If one is searching for the purest ellipsoidal variations, one should observe at a wavelength where the secondary star provides the majority of the systemic luminosity. In the optical, the accretion disk and hot spot can contaminate, if not dominate, the system luminosity. Even in quiescence, there could be a modest amount of dilution of the optical light curve by the accretion disk, hot spot, and/or (although somewhat less likely) heating of the secondary star due to the possibility of weak and variable accretion (Shahbaz, Naylor, & Charles 1997). On the other hand, in the infrared, the late type secondary stars can dominate the quiescent binary's luminosity. This reduces the uncertainties in modeling the system. For V616 Mon, MRW find that the K star contributes

$83\pm4\%$  in the blue, and  $94\pm3\%$  of the continuum flux near  $H\alpha$ . This percentage should be even higher at longer wavelengths. Therefore, observations in the infrared will reveal more genuine ellipsoidal variations than observations in the optical regime.

SNC and FR both observed V616 Mon in the infrared. SNC obtained a  $K$ - band light curve, while FR obtained  $H$ - band light curves as well as much more sparsely sampled  $J$ - and  $K$ - band curves. Neither study could accurately determine the amount of contamination present from other sources of light in the system. Because of this, the orbital inclination angle determined from FR spanned nearly the entire range of published results ( $38^\circ \leq i \leq 75^\circ$ ). In order to determine if contamination is present, multi-wavelength observations are needed.

Currently, the best way to obtain the orbital inclination angle in non-eclipsing binary systems is to model the ellipsoidal light curves. Previously published inclination angles for V616 Mon range from  $31^\circ$  (lower limit from SNC) all the way to  $75^\circ$  (upper limit from FR). These angles correspond to primary masses of  $28.8 M_\odot$  to  $3.3 M_\odot$ , respectively. The large range in derived inclination angles (and masses) appears to be due in part to the changing shape of the observed light curves over time. In 1986 December and 1987 January, HRHSA saw evidence for a “grazing eclipse of the Roche lobe-filling star by the accretion disk”, but when MRW observed the SXT in 1991 December and 1992 January, this feature was no longer present. If the eclipse was real, it would indeed suggest a high orbital inclination angle. However, no other published data on V616 Mon has shown evidence for such events. The most recently published data set on V616 Mon was taken by FR in 1995 and 1996. The data showed that as the  $H$ - band light curve shape exhibited slight changes over the one year baseline of their observations, the mean  $H$  magnitude remained constant.

We have undertaken a program to attempt to determine more precise orbital inclination angles and primary masses for five SXTs. We have observed these SXTs in the infrared, and have already presented results on GU Mus (Paper 1). We now present our results for the prototype SXT, V616 Mon, based on a two year baseline of multi-wavelength optical and infrared observations. We model these data with both WD98, as done in Paper 1, and independently with the ELC code (Orosz & Hauschildt 2000). In section 2, we describe our observations and data reduction process. In section 3, we present our infrared photometric light curves and discuss the possibility of long and short term variability. Section 4 describes our choices for the relevant input parameters for WD98 and ELC. We present the resulting models at  $J$ ,  $H$ , and  $K$ , and discuss the possible scenarios to explain the changing shape of the long-term light curves. Finally, in Section 5 we discuss the implications of the models, and compare our results to those previously published.

## 2. Observations & Data Reduction

We obtained infrared photometry of V616 Mon on three separate epochs over a 22.5 month interval. We first observed the SXT prototype using GRIM II<sup>4</sup> on the Astrophysical Research Consortium 3.5-m telescope at Apache Point Observatory on 1999 February 25. We then used IRIM<sup>5</sup> on the 2.1-m telescope at the Kitt Peak National Observatory on 2000 February 12 and 16, and had our third and final observing run on the same telescope using SQUIID<sup>6</sup> on 2000 December 8, 9, and 11.

On 1999 February 25, V616 Mon was observed from 3:43 to 7:41 UT with the camera at the f/5 plate scale ( $0''.473 \text{ pixel}^{-1}$ ). With an orbital period of about 7.75 hours, this first observing session covered just over half of an orbital period. Photometric data were obtained in the GRIM II  $J$  ( $\lambda_c = 1.265\mu\text{m}$ ) filter. Our observing sequence consisted of two 15 second images at one position, a beam switch, and two additional 15 second images. All of the data were linearized with an IRAF linearization task written by A. Watson (1996, Private Communication). After averaging the two images at one position, we subtracted them from the average of the two images at the other position. These sky, and bias-subtracted images were then flat fielded with a sky flat using the usual IRAF packages.

V616 Mon was observed again on 2000 February 12 from 4:16 to 6:41 UT and on February 16 from 1:45 to 8:06 UT with the camera at the f/15 focus ( $1''.09 \text{ pixel}^{-1}$ ). This second observing run effectively covered one orbital period. Data were obtained in the IRIM  $J$  ( $\lambda_c = 1.24\mu\text{m}$ ),  $H$  ( $\lambda_c = 1.65\mu\text{m}$ ), and  $K'$  ( $\lambda_c = 2.16\mu\text{m}$ ) filters. Our observing sequence was the same as that for the GRIM II data. We began with the  $K'$  filter, refocussed and switched to the  $H$  filter, and repeated the procedure for the  $J$  filter before returning back to the  $K'$  filter and refocussing again. Each individual  $J$  image consisted of 1 frame of 30 seconds, the corresponding  $H$  images consisted of 6 coadded frames of 8 seconds each, while each  $K'$  image consisted of 10 coadded frames of 4 seconds each. We processed the images as above, this time linearizing the data using the IRLINCOR package in IRAF with the coefficients supplied in the IRIM User’s Manual.

We observed V616 Mon for the final time on 2000 December 8 from 4:59 to 12:29 UT, on December 9 from 4:36 to 12:34 UT, and on December 11 from 6:42 to 12:18 UT, all with the camera at the f/15 focus ( $0''.69 \text{ pixel}^{-1}$ ). This final observing run covered 2.72 orbits. Data were obtained in the SQUIID  $J$  ( $\lambda_c = 1.267\mu\text{m}$ ),  $H$  ( $\lambda_c = 1.672\mu\text{m}$ ), and  $K$  ( $\lambda_c = 2.224\mu\text{m}$ ) filters. This time, we observed with an ABBA sequence. SQUIID stands for “Simultaneous Quad Infrared Imaging Device”, and takes images in 4 filters simultaneously. Due to this, the number of coadds and exposure times for each filter had to be identical. Each individual image consisted of 8 coadded

---

<sup>4</sup>See <http://www.apo.nmsu.edu/Instruments/GRIM2/>

<sup>5</sup>See <http://www.noao.edu/kpno/manuals/irim/>

<sup>6</sup>See <http://www.noao.edu/kpno/squid/squidmanual.html>

frames of 7 seconds each. We chose this exposure time to stay safely below the non-linear regime of the chip since detailed linearization curves do not yet exist for this newly commissioned instrument. Dome flats were taken due to the long readout time per exposure. We again processed the images as above with IRAF.

For each of the three data sets, we performed aperture photometry on V616 Mon and the same five nearby field stars. Using the IRAF PHOT package, a differential light curve in each wavelength regime was generated with each point being the average of four beam switched images. For the GRIM II and SQUID data sets, our differential photometric results show that over the course of our observations, the comparison stars did not vary more than expected from photon statistics. Unfortunately, while the S/N of the IRIM data set was high ( $\sim 1\%$  relative photometry), these data showed considerable scatter due to very good seeing which resulted in the undersampling of the PSF.

Optical observations of V616 Mon were taken with the Cassegrain Focus CCD Imager<sup>7</sup> on the 0.9 meter telescope at CTIO on 2001 March 15 at 00:50 UT. Data were obtained in the  $B$ ,  $V$ ,  $R$ , and  $I$  bandpasses for the purpose of determining the quiescent optical colors of the system. The 180 second exposures (300 seconds for the  $B$  band) were zero corrected and flat fielded before aperture photometry was performed. Standards were also observed to transform these data to the system of Landolt. The observed optical and infrared colors of V616 Mon can be found in Table 1, along with previously published optical colors for this system.

### 3. Long and Short Term Variability of the Light Curve

Since the 1975 outburst of V616 Mon, several variations of light curve shape have been observed. A few years after the system's transition into its quiescent state, McClintock & Remillard (1986) obtained " $B + V$ "- and  $I$ - band light curves. In both of these light curves, the deeper minimum coincided with the inferior conjunction of the secondary star. When HRHSA observed the system in 1986 and 1987, the deeper minimum instead corresponded to the inferior conjunction of the primary object. In 1990, Bartolini et al. (1991) obtained a light curve with minima consistent with HRHSA's, but their brightest maximum was observed to be shifted by 0.5 in phase. Similar changes were found by Leibowitz, Hemar, & Orio (1998) when they studied the  $R$ - band light curve of V616 Mon over a seven year period. They found that not only did the shape of the light curve change over time, but also the mean brightness of the system seemed to vary on a time-scale of hundreds of days with a peak-to-peak amplitude of 0.3 mag. More recently, FR saw evidence for a slightly changing  $H$ - band light curve shape over a one year baseline of observations. However, they did not see any sharp dips or asymmetry reversals between the two light curve maxima. In addition, the mean  $H$ - band magnitude remained fairly constant over the course of their observations.

---

<sup>7</sup>See <http://www.ctio.noao.edu/cfcd/cfcd.html>

With the history of V616 Mon’s changing light curve shape, we were interested in determining its current level of activity. We observed V616 Mon over a roughly two year period including three nights in December 2000. In Figure 1, we present the  $J$ -,  $H$ -, and  $K$ - band light curves of V616 Mon obtained on 2000 December 8, 9, and 11. The data were phased to the Leibowitz, Hemar, & Orio (1998) ephemeris, and then shifted by 0.5 in phase so phase 0.0 corresponds to the inferior conjunction of the secondary star (where the secondary star is in front of the black hole from the viewpoint of the observer). Each symbol represents a different night of observations. There are no strong variations in the amplitude or mean brightness of the SXT from night to night. This indicates that the infrared light curves are stable over time periods of days. Since each night of observation revealed a light curve shape consistent with the other two, we binned the points in a given phase interval and combined the three nightly light curves into one for each wavelength regime. The results are presented in Figure 2. Our infrared light curves most closely resemble the optical light curves of HRHSA, with the brighter maximum occurring at phase 0.25 and deeper minimum at phase 0.5. If we compare our  $H$ - band light curve to FR’s, we find that the deeper minimum occurs at phase 0.5 in both curves, but the brighter maximum differs by 0.5 in phase.

Since the shape of our 2000 December light curves differed from FR’s taken in 1995 and 1996 (the  $H$ - band magnitudes were consistent within the errors), we utilized our almost two year baseline of observations to investigate if the shape of the light curve had changed over this time. Figure 3 presents the  $J$ -,  $H$ -, and  $K$ - band light curves phased as in Figure 1. Unfortunately, while the S/N of the IRIM data set (filled triangles) was high ( $\sim 1\%$  photometry), these data showed considerable scatter due to very good seeing which resulted in the undersampling of the PSF. In any case, both the shape and brightness of the observed light curves are consistent over the period of observations. Nonetheless, the evidence for long-term changes in the shape of the quiescent light curves of V616 Mon is interesting, and we will return to this subject in the next section.

## 4. Modeling the Infrared Light Curves of V616 Mon

We adopt as our light curves the binned  $J$ -,  $H$ -, and  $K$ -band light curves from 2000 December (Figure 2). In order to find the inclination of the binary, we conducted two more or less independent analyses of these data, which we describe below.

### 4.1. Basic Models and Assumptions

#### 4.1.1. Assumed Secondary Star Parameters

For multi-wavelength light curve modeling, the most important input parameters are based on the temperature of the secondary star. In 1977, Oke detected a cool spectrum from the source and attributed it to a K5V - K7V star. HRHSA’s analysis of V616 Mon favored a spectral type of

K3 - K4. Shahbaz, Bandyopadhyay, & Charles (1999) compared their observed  $K$ -band spectrum of V616 Mon to the spectra of comparison stars of spectral types K0V, K3V, K5V, and K7V, and using  $\chi^2$  tests, determined a best fit spectral type of K3V for the secondary star. Here, we examine multi-wavelength photometry to estimate the secondary star’s spectral type.

Table 1 presents the post-outburst infrared and optical colors of V616 Mon. The mean colors are consistent with those of a K4V star reddened by  $A_V = 1.21$  mag (Wu et al. 1976; Seaton 1979,  $E(B - V) = 0.39$ ). In Figure 4 we compare the dereddened observed spectral energy distribution (SED) of V616 Mon to a K4V star (Bessell & Brett 1988; Cousins 1976; Johnson 1966; Mikami & Heck 1982). Except at  $B$  and  $J$ , the two sets of data (normalized at  $H$ ) are consistent within the errors. Based on the photometry, there is evidence for excess light at  $B$  (22%) and a possible small excess at  $J$ . This  $B$ -band excess is consistent with that found by MRW, and helps us to constrain the amount of contamination by the accretion disk and/or hot-spot. Based on the mean observed colors of V616 Mon, and its resulting spectral energy distribution, we adopt a spectral type of K4 for the secondary star. We adopt as the corresponding temperature a value of  $T_{\text{eff}} = 4600$  K (Johnson 1966).

Given that the photometry and optical/infrared spectroscopy agree, the simplest assumption is that the K4 secondary star dominates the  $VRIJHK$  luminosity of the system. We can, however, envision scenarios (some of which are highly tuned) where a K-type SED might be mimicked by accretion processes. Without accurate models for the spectra of quiescent SXT accretion disks, we can not further speculate on the exact level of contamination associated with these processes and therefore assume that nearly all of the infrared light in the system comes from the secondary star.

The secondary stars in systems such as SXTs can have masses and radii that do not correspond to accepted values for main sequence stars. In addition, some of these stars have been found to have parameters consistent with those of evolved stars (e.g. Paper 1). Mass estimates range from that of a zero-age main sequence star (ZAMS) to those of a less massive subgiant (Iben, Tutukov, & Fedorova 1997, MRW). Fortunately, we do not need a value for the mass of the secondary star as long as we have a good measurement for the mass ratio,  $q$ . Unlike GU Mus (Paper 1), V616 Mon has a well determined mass ratio. MRW measured the mean rotational velocity of the secondary star. Their value of  $v \sin i = 83 \pm 5$  km s $^{-1}$  implies a mass ratio of  $q \equiv M_2/M_1 = 0.067 \pm 0.01$ , assuming the secondary star is rotating synchronously with the orbit. It turns out that the derived orbital inclination angle is relatively insensitive to the value of  $q$ ; however,  $q$  will be important in the determination of the primary object’s mass once the orbital inclination angle is known.

#### 4.1.2. WD98 Model Setup

The first of the models used was WD98, the newest version of the Wilson-Devinney light curve program (Wilson 1998, J. Kallrath 1999, private communication; R. E. Wilson 1999, private communication). See Paper 1 for references and a basic description of the code. We ran WD98 in a

mode for a semi-detached binary with the secondary star automatically filling its Roche lobe (Mode = 5), and the primary having such a large gravitational potential, that it essentially has zero radius. The secondary star atmosphere was determined from solar metallicity Kurucz models. See Paper 1 for a discussion of the parameters such as limb darkening, gravity darkening, and bolometric albedo. The most important wavelength-independent input values to WD98 are listed in Table 2, and the wavelength-dependent parameters in Table 3 (units are shown where appropriate). Since any realistic hot spot or disk contamination for this system will have a minimal heating effect on the secondary star (HRHSA; FR), we have used normal, non-irradiated, limb darkening coefficients in our models. In addition, we adopt the gravity darkening exponent found by Claret (2000) for a K4 star ( $T_{\text{eff}} = 4600$  K):  $\beta_1 = 0.40$  (Table 2).

We did not make use of the optimizer program supplied with WD98. It proved to be much more convenient to simply compute large grids of models and use a simple program to compute  $\chi^2$  values of the fits. The mass ratio was usually fixed at its spectroscopic value. In order to quantify the sensitivity of the models to the variations of the input parameters, we ran models with inputs covering a wide range of parameter space as in Paper 1. We found that the best fit orbital inclination angle did not change significantly as we varied the temperature of the secondary star by one spectral type. Varying  $q$  from 0.057 to 0.077 (the  $1\sigma$  error bars from MRW), also had no effect on our final orbital inclination angle.

#### 4.1.3. ELC Model Setup

The second code we used was the ELC program, which is fully described in Orosz & Hauschildt (2000). In its “black body” mode ELC is essentially the same as modes 2, 4, 5, and 6 of WD98. ELC has at least two features with no direct analog in WD98. The first is the (optional) inclusion of a flared accretion disk around “star #2”. The second is the way in which model atmosphere intensities are included in the model. WD98 tabulates the ratios of solar metallicity model atmosphere intensities to black body intensities for surface normals (i.e. a viewing angle of  $\mu = 1$ ). The intensities for other viewing angles are computed using the specified limb darkening law (a single limb darkening law is used for the entire star). ELC tabulates model solar metallicity atmosphere specific intensities (Hauschildt, Allard, & Baron 1999a; Hauschildt et al. 1999b) as a function of three parameters, namely the effective temperature, the surface gravity, and the viewing angle  $\mu$ . Hence no parameterized limb darkening law is needed. For stars with large surface gravities ( $\log g > 3.5$ ) the systematic differences between ELC and WD98 are quite small (less than  $\approx 1\%$ ). However, for cool giants, the differences in the light curves can be dramatic (Orosz & Hauschildt 2000).

ELC currently has four different optimizer routines with various levels of sophistication. They are the “grid search” method and a Levenberg-Marquardt routine adapted from Bevington (1969), a routine which uses the downhill simplex method (essentially the “amoeba” routine from Press et al. 1992), and a genetic algorithm based on the “pikaia” routine given in Charbonneau (1995). The



genetic routine proved to be by far the most useful routine here. The three basic free parameters of the model are the mass ratio, the inclination, and the orbital separation. The binary observables that were modeled were the three infrared light curves, a simulated velocity curve with  $K_2 = 433 \pm 3$  km s<sup>-1</sup> (MRW), and MRW’s value of the mean rotational velocity of the secondary star ( $83 \pm 5$  km s<sup>-1</sup>). The optimization routines attempt to find a parameter set so that the total  $\chi^2$  is minimized ( $\chi_{\text{total}}^2 = \chi_{\text{light}}^2 + \chi_{\text{velocity}}^2 + \chi_{\text{rotation}}^2$ ).

#### 4.2. Simple Ellipsoidal Models of the Secondary Star

We first ran models assuming the secondary star was the sole source of light. Aside from limb- and gravity- darkening effects, the secondary star was assumed to have a uniform surface brightness.

The WD98 models were run for a range of inclination angles, using the input parameters listed in Tables 2 and 3. The best fit was determined based on  $\chi^2$  tests. In Figure 5, we present our 2000 December V616 Mon *J*-, *H*-, and *K*- band observations and the corresponding WD98 model (solid line) for the best fit value of the orbital inclination angle  $i = 40^\circ$ .

Three iterations of the ELC grid search program were used to fit the data and the results are shown as the dashed line in Figure 5. The fitted parameters are  $i = 40.03^\circ$ ,  $q = 0.0604$ , and  $a = 4.543 R_\odot$ . The WD98 and ELC models are nearly indistinguishable.

It is clear that the infrared variations we observed are not purely ellipsoidal. All three light curves reveal a small difference between the two maxima, as well as a small deviation ( $\sim 3\%$  at *K*) between phases 0.0 and 0.25. There are several possible explanations that could account for this light curve shape, and we discuss them in the following sections.

#### 4.3. Possible “Contamination” Scenarios

There are two main effects that could result in a phase dependent deviation from ellipsoidal variations. These possibilities are direct light from a hot spot on the edge of the accretion disk, and spots on the secondary star, either cool (dark) or hot (bright) spots. The long-term changing shape of the light curves discussed in Section 3 may be explained if the level of heating or the positions of these spots vary over time. We will consider each of these possibilities in turn.

##### 4.3.1. A Migrating Accretion Disk Hot-Spot

In 1991, MRW “imaged” V616 Mon through doppler tomography, and found evidence for a hot spot on the accretion disk. The hot spot is presumably formed when the accretion stream from the

secondary star impacts the accretion disk. The accretion stream has a predicted path, therefore, in order for the hot spot to migrate around the edge of the disk, the disk size must change. There have been suggestions that the accretion disk in V616 Mon has changed in size over the past two and a half decades. For example, based on the change in the peak separation of observed  $H\alpha$  lines between 1991 and 1993, and its corresponding change in the disk velocity ( $\Delta V = 100 \text{ km s}^{-1}$ ), Orosz et al. (1994) suggested that the accretion disk had contracted. Thus, the accretion disk may indeed change in size causing the hot spot to migrate. The hot spot could introduce a phase dependent source of light if the accretion disk was optically thick. If the spot were more or less on the disk rim, then its viewing angle would change considerably over the orbit, giving rise to a phase-dependent modulation.

We investigated several spotted disk models using ELC and its genetic code. There are several extra parameters needed to describe the disk. They are the inner and outer radii, the opening angle of the outer edge, the temperature at the inner edge, and the power-law exponent which describes the temperature profile. In addition, four parameters are needed for a spot. They are the azimuth angle, the angular size of the spot, its radial extent, and its “temperature factor”. About 30,000 models using a wide range of input parameters were computed and fitted using the genetic code. In the end we found what FR had found, namely that one can find models with a wide range of inclinations that give nearly equally good fits. In our case the inclinations ranged from about 40 degrees to 60 degrees with a change in the total  $\chi^2$  of less than 1. Fortunately, with the use of multi-color photometry and the observed spectral energy distribution, we are able to exclude a large number of these models. These models generally predict that on the order of 50% of the light in the infrared should come from the accretion disk. The “disk fraction” in the optical is predicted to be even larger. The ultra-violet to infrared SED of V616 Mon (Figure 4) limits the excess light from the accretion disk and hot-spot to 22% at  $B$ , and  $\leq 3\%$  at all other visible and near-infrared wavelengths. Although we cannot rule out up to a  $\approx 3\%$  level of diluting infrared light from the accretion disk and/or hot spot, we can certainly rule out the large dilutions predicted by the spotted disk models. Based on these arguments, we do not believe that direct light from the hot-spot is the cause of the excess in the ellipsoidal variations.

#### 4.3.2. *Star Spots*

Star spots are believed to be common features on many late-type stars. Their colors will not be drastically different from a K4V star, and therefore do not significantly alter the observed SED. Spots on late-type stars typically vary on timescales of months to a few years (Bouvier & Bertout 1988; Vogt 1975). McClintock & Remillard (1990) state that changes in the brightness of the star by up to 0.2 magnitudes are possible from spots alone. The variation in the  $V$  magnitude reported since the SXT’s return to quiescence has spanned about 0.17 magnitudes (see Table 1). Shahbaz, Naylor, & Charles (1994) found that for spots that are about 750 K below the effective temperature of the star, the amplitude of the spot modulation is about half as much in the infrared

as in the visual. They find a 3% modulation in the  $K$ -band for spots similar to those found on RS CVn stars that cover about 8% of the star. We also see a 3% difference in our  $K$ -band maxima. Khruzina & Cherepashchuk (1995) applied a model of a spotty Roche lobe filling star to explain the anomalies in and the long-term variability of the V616 Mon light curves. They found that they could explain all of the peculiarities in the optical and infrared variability of V616 Mon in its quiescent state by introducing dark spots on the surface of the K-star with temperatures 10% - 40% lower than the mean stellar temperature. They successfully modeled the  $B$ -band light curves obtained by McClintock & Remillard (1986) and Bartolini et al. (1991), even though the light curves were completely different in appearance. They implemented one spot on the hemisphere facing the compact object to explain the light curve of McClintock & Remillard (1986), and two spots on the opposite hemisphere to explain the light curve of Bartolini et al. (1991). Khruzina & Cherepashchuk (1995) conclude that the spotted model is a “natural explanation of brightness’s inequality in the quadratures of both curves and temporal variations of the curves’ ratio, as well as that of the shape and depth of both minima.” The star spots they used reached a few tenths of the stellar radius, and had temperatures that were 10% - 40% lower than the mean effective stellar temperature. Finally, Bildsten & Rutledge (2000) suggested that the observed X-ray luminosity of V616 Mon could be attributed to coronal activity on the secondary star. Presumably such coronal activity would have associated spots.

Using these dark spot scenarios, we ran WD98 models with a single cool spot on the surface of the secondary star. The geometry of the WD98 model places  $0^\circ$  longitude at the line of star centers, measured counterclockwise as viewed from the “north” (+z) pole. The angular radius of the spot corresponds to the angle subtended by the spot radius at the center of the star. With  $i = 40^\circ$ , we varied the latitude of the spot from  $45^\circ$  to  $135^\circ$  ( $45^\circ$  on either side of the equator), the longitude of the spot from  $90^\circ$  to  $162^\circ$  (on the leading side of the star), the radius of the spot from  $60^\circ$  (44% coverage) to  $9^\circ$  (2% coverage), and the temperature of the spot from 4100 K to 3000 K. The best fit  $\chi^2$  value came from the model of a 3600 K spot centered directly on the equator and at a longitude of  $135^\circ$ , with a radius of  $18^\circ$  (4% coverage). The model is plotted as a solid line in Figure 6. Of course, this same model could be generated by several spots, or groups of spots, that have the same average parameters as the model presented here.

An alternative source of phase-dependent contamination is to have parts of the star brighter than they would otherwise be, either due to stellar activity (i.e. similar to the faculae on the Sun), or possibly due to heating of the star by a disk hot spot. With  $i = 40^\circ$ , we varied the hot spot temperature from 4646 K to 4800 K, the spot latitude from  $45^\circ$  to  $135^\circ$  ( $45^\circ$  on either side of the equator), the spot longitude from  $240^\circ$  to  $342^\circ$  (on the trailing side of the star), and the spot coverage from 100% (spot radius =  $90^\circ$ ) to 30% (spot radius =  $50^\circ$ ) of one hemisphere of the star. The best fit model was again determined from  $\chi^2$  tests. While several models had very low  $\chi^2$  values, the model with the lowest value had a 4715 K spot that covered 100% of the hemisphere centered directly on the equator and at a longitude of  $315^\circ$ . Models with smaller spots ( $\geq 60\%$  coverage) and temperatures varying from 4646 K to 4738 K gave slightly higher  $\chi^2$  values.

For example, a 4681 K spot centered at the same longitude and latitude that covered 64% of the hemisphere had a  $\chi^2$  value that was 0.02 higher than that of the best fit model.

We also used ELC and its genetic code to explore spotted star models. The spot parameters are used in the same way as in WD98. Several populations were evolved, allowing for either a hot or a cool spot. Roughly 120,000 models and fits were computed. In general, compact hot spots (with typical angular radii of 10 degrees) on the trailing face of the star or larger cool spots (with radii of up to 90 degrees) near the leading face of the star provided good fits. The cool spot model with the best  $\chi^2$  is shown as the dashed line in Figure 6. This model has  $i = 40.88^\circ$ ,  $q = 0.0654$ ,  $a = 4.157 R_\odot$ . The 3495 K cool spot is centered at a latitude of  $172.4^\circ$ , and a longitude of  $0.1^\circ$ , and has an angular radius of  $86.8^\circ$ . The hot spot model with the best  $\chi^2$  has  $i = 41.56^\circ$ ,  $q = 0.0628$ ,  $a = 4.404 R_\odot$ . With a 9050 K spot at a latitude of  $83.4^\circ$ , a longitude of  $171.1^\circ$ , and an angular radius of 7.9 degrees.

Could these hot spots be “intrinsic” to the star, or could the star be externally heated? The best fit WD98 model has the entire trailing hemisphere of the star slightly hotter than the leading hemisphere. This type of temperature distribution may be explained by external heating of the secondary star. One major problem for the external heating scenario, however, is that there is little evidence for a *luminous* hot spot on the accretion disk which could act as the source of heating. McClintock & Remillard (2000) report a low UV flux. A blackbody of 12000 K fits the dereddened UV points from McClintock & Remillard (2000) fairly well, and explains the 22% contamination at  $B$ . When the blackbody is added to the flux for the K4V (open triangles in Figure 4), it nicely accounts for the differences between the K4V SED and the observed SED of V616 Mon. Based on the total flux of the blackbody and the distance to V616 Mon, the radius of the blackbody area is  $0.05 R_\odot$ . This amounts to roughly 2.5% of the radius of the accretion disk if the disk fills half of its predicted Roche lobe. If this black body is used to represent the hot spot on the disk, these results suggest that the hot spot temperature is about 12000 K, consistent with hot spot temperatures found for cataclysmic variable disks (Hoard & Szkody 1996). We also attempted to fit the observed UV data with a 9000 K blackbody, as found in McClintock, Horne, & Remillard (1995), however, the 12000 K blackbody better explained the data. Is this hot spot luminous enough to heat the star the required amount to explain the observed light curves? According to Brett & Smith (1993), if the irradiated atmosphere is assumed to adopt the structure of a hotter star with an effective temperature  $T'_{\text{eff}}$ , then  $\sigma T'^4_{\text{eff}} = \sigma T^4_{\text{eff}} + w F_{\text{inc}}$  where  $F_{\text{inc}}$  is the flux incident upon the star being heated. In order to determine the most favorable case for a heating scenario, the value of  $w$  is taken to be 1 here (the normal value is approximately 0.5). To raise the temperature of the star from 4600 K to 4715 K, a flux of  $2.63 \times 10^9 \text{ erg s}^{-1} \text{ cm}^{-2}$  is needed. A 12000 K hot spot with a  $B$  magnitude that is equal to 22% of the dereddened  $B$ -band flux, can not be more than  $0.86 R_\odot$  ( $0.25 R_{L1}$ ) away from the secondary star in order to heat it by 115 K. To heat the star by 81 K, the accretion disk hot spot can not be more than  $1.211 R_\odot$  ( $0.35 R_{L1}$ ) away from the secondary star. These solutions require a disk radius of 0.65 to  $0.75 R_{L1}$ , while the system probably needs a much smaller disk in order to allow the accretion stream to travel around it to the “back side”

before impacting the disk. Unless the phasing of Leibowitz, Hemar, & Orio (1998) is off by  $180^\circ$ , the heating model seems unlikely.

The best fit ELC hot spot model places a small 9050 K spot near the equator on the end of the star opposite from the  $L_1$  point. Since it is unlikely that such a spot could be a result of external heating, we explore the possibility of faculae on the secondary star. Solar faculae are found around groups of sunspots and are normally visible near the limb of a star. The lifetime of an average solar faculae is about 15 days, while that of a large faculae which dominates solar variations can last almost three months (Chapman & McGuire 1977). Since individual star spots can exist for much longer timescales than their solar counterparts, it may be possible for stellar faculae to also exhibit much longer lifetimes. However, even though it may be possible for faculae to remain stable over the baseline of our observations, they do not appear to be able to account for a spot that has a temperature of almost twice that of the effective temperature of the star. Chapman & McGuire (1977) find that in general, the facular contrast has a  $\lambda^{-1}$  dependence. “White light” faculae on the sun are associated with bright regions, but in the infrared, they appear darker than the quiet photosphere (Foukal, Little, & Mooney 1989). It does not appear as though faculae on the secondary star in V616 Mon could have parameters consistent with the ELC hot spot.

#### 4.4. The Adopted Model and its Uncertainties

Given the plausibility of the physical nature of the dark spots, and their ability to reproduce light curves of vastly differing shapes through migration, we suggest that cool spots on the surface of the secondary star are the cause of the phase dependent deviations in the ellipsoidal variations seen in the  $J$ -,  $H$ -, and  $K$ - band light curves. From the SED shown in Figure 4, we adopt a model that has no light from an accretion disk.

The best fitting inclination from the WD98 models is  $i = 40^\circ$  and from the ELC models is  $i = 41.5^\circ$ . Based on errors in the amount of infrared diluting light in the system, and the ability of the  $\chi^2$  tests to distinguish between model fits to the observed data, the uncertainty in the WD98 value is about 1.5 degrees. The ELC code and its genetic routine provide an easy way to estimate the uncertainties on the fitted parameters, especially the inclination. We simply plotted the  $\chi^2$  values as a function of the inclination and looked to see how the value of  $\chi^2$  changes near the minimum. Figure 7 shows the “lower envelope” of the  $\chi^2$  values as a function the inclination, which is basically the smallest  $\chi^2$  value within each  $0.1^\circ$  bin. The  $\chi^2$  values were scaled to give  $\chi^2_{\text{nu}} = 1$  at the minimum. Although not all bins are filled, it appears that the *formal* statistical uncertainty in the inclination is rather small, on the order of  $2^\circ$  or so. We estimate that the systematic error caused by contamination of disk light at the few percent level is on the order of  $1^\circ$ . We adopt as our final inclination  $i = 40.75 \pm 3^\circ$ .

Our derived orbital inclination angle is inconsistent with HRHSA’s, but agrees with SNC’s inclination determined from their  $K$ -band light curve of V616 Mon. We do not see any evidence

for an accretion disk hot spot affecting the infrared light curves, and thus our results differ from those of FR.

## 5. Discussion

With the excellent match of the observed photometry with a K4V SED, we find that the optical and infrared contamination from a constant source of light in the system is  $\leq 3\%$ , with an exception at  $B$ . Combining HST UV observations (assuming a 12000 K blackbody for the hot spot on the accretion disk), we can explain the observed SED from the ultraviolet to the infrared. We first ran models for an uncontaminated K4V star and found a best fit orbital inclination of  $40^\circ$ . This model could not fit the unequal maxima of the infrared light curves, as a purely ellipsoidal model exhibits equal maxima. In order to determine the phase dependent nature of the ellipsoidal deviations in the V616 Mon light curves, we have considered three possibilities. We ruled out models for a migrating hot-spot on the accretion disk based on the low level of optical and infrared diluting light in the system. However, models with either cool spots or hot spots on the surface of the star fit the data nearly equally as well, although the heated spot model was slightly better. However, each model has its own problems.

There are several main problems with the heated face models. Firstly, the heated part of the star is the trailing hemisphere. This means that the hot spot needed to heat it would have to be on the opposite side of the accretion disk than is normally expected. Secondly, the heating mechanism must be uncomfortably close to the secondary star in order to heat it and explain the data. There does not appear to be sufficient luminosity in the system to heat the star from the suggested distance of a hot spot on the accretion disk ( $0.5 R_{L1}$ ). This scenario might work if the phasing were to be off by  $180^\circ$  (but this possibility seems unlikely).

Contrary to the heated models, the dark spot models seemed to be physically viable, but even these models had their own peculiarities. The best fit WD98 dark spot models placed the spot directly on or very close to the equator. Also, the model had one spot on the leading face of the secondary star. Thus this model may require a special scenario, however it is likely that this same model could be generated by multiple spots that have the same average parameters. Nonetheless, this model is consistent with both the long-term as well as current observations of V616 Mon. Spots are presumed to be a natural occurrence on the surfaces of late-type stars. Any such spots, however, must be nearly unchanging on multi-year timescales. Dark spots have also been used to explain the changing light curves of Cen X-4 (McClintock & Remillard 1990) as well as other binary systems. Detailed long-term monitoring of V616 Mon and other SXTs should prove extremely useful in determining the behavior of spots (if present) on long timescales.

With the orbital inclination angle determined as  $i = 40.75 \pm 3^\circ$ , we can estimate the mass of the primary and other interesting parameters. The other observed quantities that are needed for this exercise are the (projected) radial velocity and rotational velocity of the secondary star

( $K_2 = 433 \pm 3 \text{ km s}^{-1}$  and  $v \sin i = 83 \pm 5 \text{ km s}^{-1}$ , MRW), and the orbital period ( $P = 0.323016$  days, McClintock & Remillard 1986). The ELC code was used to numerically find the relationship between  $K_2$ ,  $v \sin i$ , and the mass ratio  $q$ , and a simple Monte Carlo code was used to compute the uncertainties on the binary system parameters, assuming the quoted uncertainties on all of the input values above are  $1\sigma$ . We find a black hole mass of  $11.0 \pm 1.9 M_\odot$  and a mass of  $0.68 \pm 0.18 M_\odot$  for the secondary star. Note that this mass is consistent with that of a “normal” K4V (Gray 1992).

The distance to the source depends on its luminosity and extinction. We used the synthetic photometry computed from the NEXTGEN models<sup>8</sup> to compute the expected absolute  $J$ ,  $H$ , and  $K$  magnitudes of the star from its temperature, radius, and surface gravity. For this exercise we adopt a  $1\sigma$  error on the effective temperature of 200 K, which is roughly one subclass in K (Gray 1992). We used the color excess of  $E(B - V) = 0.39 \pm 0.02$  given by Wu et al. (1976), and extinction law of Cardelli, Clayton, & Mathis (1989) to find the extinctions in the three bands, assuming  $A_V = 3.1E(B - V)$ . Using our infrared photometry (Table 1) and the quoted  $1\sigma$  errors, we used another simple Monte Carlo procedure to compute the absolute magnitude and the distance modulus and their uncertainties in each of the  $J$ ,  $H$ , and  $K$  filters. The results are summarized in Table 4. Our adopted value of the distance is the simple average of the distances derived for the three filters:  $d = 1164 \pm 114 \text{ pc}$ . This distance is consistent with that found by SNC ( $660 \leq d \leq 1450 \text{ pc}$  with the most probable value at 1050 pc).

In order to understand the outbursts of SXTs, we need to be able to model them with refined input parameters. As discussed in Paper 1, the orbital inclination angle can play an important role in the appearance of an SXT outburst. Esin et al. (2000) used a black hole mass of  $4.5 M_\odot$ , an orbital inclination angle of  $i = 65^\circ$ , and a distance of 1.4 kpc as inputs to their advection dominated accretion flow (ADAF) models. While the distance they used was close to the one we find here, the black hole mass and inclination angle are not. Any new models that are constructed to explain the outburst of V616 Mon should take into account our results for the mass of the black hole, the orbital inclination angle, and the distance.

We assumed that the accretion disk contributes essentially no light in the infrared. Based on this assumption, we adopted a value of the inclination of  $i = 40.75^\circ$ . As the SED in Figure 4 shows, there are good reasons to think that this assumption is valid. Given how critical this assumption is (i.e. a disk contamination of 50% would drive the inclination up to around  $60^\circ$ ), it would be extremely worthwhile to test it in as many ways as possible. Shahbaz, Bandyopadhyay, & Charles (1999) obtained a  $K$ -band spectrum of the source with modest resolution ( $47 \text{ \AA}$  FWHM) and signal-to-noise ( $\approx 30$ ) and concluded that the  $2\sigma$  upper limit on the accretion disk contamination is  $\leq 27\%$  in the  $K$ -band. FR, however, criticized this result on the grounds that template stars with inappropriate surface gravities were used and that an inappropriate spectral feature (the  $\lambda 2.29 \mu\text{m}$   $^{12}\text{CO}(2,0)$  bandhead) was used. It should be relatively easy to obtain a much better infrared spectrum using the latest generation of infrared spectrographs available on the 8 to 10

---

<sup>8</sup><ftp://calvin.physast.uga.edu/pub/NextGen/Colors/>

meter class telescopes. One could observe a wider variety of templates, and also make use of the increasingly detailed spectral models for cool stars (for example the NEXTGEN models discussed in Leggett et al. 2001) to derive a more definitive upper limit on the disk contamination in the infrared.

The shape of the X-ray outburst light curves of V616 Mon and GU Mus are very similar [as can be seen in Figure 1 of King, Harrison, & McNamara (1996)] with one main difference, the time of their secondary maxima. The light curve of V616 Mon began the rise to its second X-ray maximum about 40 days after its initial outburst, while the light curve of GU Mus shows this rise beginning about 60 days afterward. Both secondary maxima lasted for about 30 days. Based on the orbital period and radial velocity of the secondary star, the GU Mus system ( $P = 10.38$  hr;  $K_2 = 406 \pm 7$  km s $^{-1}$ ) is larger than the V616 Mon system ( $P = 7.75$  hr;  $K_2 = 433 \pm 3$  km s $^{-1}$ ). V616 Mon has a larger primary mass ( $M_{1,\text{Mon}} = 11.0$ ,  $M_{1,\text{Mus}} = 6.95$ ), and we see it at more of a face-on angle ( $i_{\text{Mon}} = 40.75^\circ$ ,  $i_{\text{Mus}} = 54^\circ$ ) than GU Mus. Could the larger size of the system account for the increase in time between X-ray outburst maxima, or could it be related to the mass of the black hole? Close study of more SXTs is needed before this question can be answered with any certainty.

In Paper 1, based on the comparison of optical and infrared colors, we determined a spectral type of K4 for the secondary star in the GU Mus system. The colors were intermediate to those of a K4 dwarf and giant. As discussed above, we also determine a spectral type of K4 for V616 Mon. In this case, however, the colors are consistent with those of a K4 dwarf. By Kepler’s Third Law, the ratio of the secondary stars’ Roche lobe radii is simply related to the ratio of the orbital periods:  $R_{\text{Mon}}/R_{\text{Mus}} = (P_{\text{Mon}}/P_{\text{Mus}})^{2/3} = 0.82$ . A K4V star nominally has a radius of  $0.70 R_\odot$  on the zero-age main sequence Gray (1992). Such a star would nearly fill the Roche lobe in V616 Mon ( $R_2 = 0.80 \pm 0.07 R_\odot$ ), whereas it would only fill  $\approx 80\%$  of the Roche lobe in GU Mus. Surprisingly, accurate multi-wavelength photometry appears to be somewhat sensitive to these small radius differences.

The nature of the mass distribution of stellar-mass black holes has been in question for many years now. Based on observational evidence for seven stellar black holes with low-mass companions, Bailyn et al. (1998) attempted to constrain this distribution. Using Bayesian statistics, they suggested that six of the seven systems had black hole masses clustered around  $7 M_\odot$ . The other system, V404 Cyg, was thought to be drawn from a different distribution. Models of the evolution and supernova explosions of massive stars should be able to predict the mass distribution of stellar-mass black holes. However, because of their findings, Bailyn et al. (1998) suggested considering a new underlying mechanism for the origin of the black hole mass distribution in low-mass X-ray binaries.

The mass we found for GU Mus in Paper 1 ( $M_1 = 6.95 \pm 0.6 M_\odot$ ) is consistent with, but more precise, than the mass adopted by Bailyn et al. (1998). In the case of V616 Mon, Bailyn et al. (1998) adopted a wide range of inclinations reported in the literature ( $31 \leq i \leq 70.5^\circ$ ). As a



result, the allowed range of the mass of the black hole was rather large. The more precise mass we determine for V616 Mon is well above the cluster of masses near  $7 M_{\odot}$  and falls nicely in the mass range plotted in their Figure 1 for V404 Cyg. Although the orbital period and evolutionary status of the secondary star in V404 Cyg are significantly different from V616 Mon, their similar black hole masses may say something about the amount of post-supernova mass transfer that has taken place in both these systems. The sample size of SXTs with measured mass functions has doubled since the analysis of Bailyn et al. (1998) was done, so it would be worthwhile to revisit the issue of the distribution of stellar black hole masses. Indeed, the four most recently determined SXT optical mass functions are all rather large:  $6.0 \pm 0.36 M_{\odot}$  for XTE J1118+480 (McClintock et al. 2001),  $6.86 \pm 0.71 M_{\odot}$  for XTE J1550-564 (Orosz et al. 2001),  $9.5 \pm 3 M_{\odot}$  for GRS 1915+105 (Greiner 2001), and  $7.4 \pm 1.1 M_{\odot}$  for XTE J1859+226 (Filippenko & Chornock 2001). It is likely that some of these systems will have black hole masses that are also well above the cluster of masses near  $7 M_{\odot}$ . In addition, better measurements for more of the known systems can be used to reduce the uncertainties in the mass distribution.

This research was supported by a Grant-in-Aid of Research from the National Academy of Sciences, through Sigma Xi, The Scientific Research Society. DMG holds an American fellowship from the American Association of University Women Educational Foundation. TEH wishes to acknowledge support from NASA through grant number GO-8618 from the Space Telescope Science Institute, which is operated by the Association of Universities for Research in Astronomy under NASA contract NAS 5-26555. This research has made use of the SIMBAD database, operated at CDS, Strasbourg, France, and NASA’s Astrophysics Data System Abstract Service.

## REFERENCES

- Bailyn, C. D., Jain, R. K., Coppi, P., & Orosz, J. A. 1998, *ApJ*, 499, 367
- Bartolini, C., Guarnieri, A., Piccioni, A., Solmi, L., & Teodorani, M. 1991, in *IAU Colloq. No. 129, Structure and Emission Properties of Accretion Discs*, ed. C. Bertout, S. Colin-Souffrin, J. P. Lasota, & J. Tran Thanh Van (Paris: Frontières), 373
- Bessell, M. S., & Brett, J. M. 1988, *PASP*, 100, 1134
- Bevington, P. R. 1969, *Data Reduction and Error Analysis for the Physical Sciences*. (New York: McGraw Hill)
- Bildsten, L., & Rutledge, R. E. 2000, *ApJ*, 541, 908
- Boley, F., & Wolfson, R. 1975, *IAU Circ.* 2819
- Bouvier, J., & Bertout, C. 1988, *A&A*, 211, 99
- Brett, J. M., & Smith, R. C. 1993, *MNRAS*, 264, 641
- Cardelli, J. A., Clayton, G. C., & Mathis, J. S. 1989, *ApJ*, 345, 245
- Chapman, G., & McGuire, T. 1977, *ApJ*, 217, 657
- Charbonneau, P. 1995, *ApJS*, 101, 309
- Charles, P. A. 2001, in *Black Holes in Binaries and Galactic Nuclei*, eds. L. Kaper, E. P. J. van den Heuvel, & P. A. Woudt, (Berlin: Springer), p. 27
- Claret, A. 2000, *A&A*, 359, 289
- Cousins, A. W. 1976, *MmRAS*, 81, 25
- Elvis, M., Griffiths, C. G., Turner, M. J. L., & Page, C. G. 1975, *IAU Circ.* 2814
- Esin, A. A., Kuulkers, E., McClintock, J. E., & Narayan, R. 2000, *ApJ*, 532, 1069
- Filippenko, A. V., & Chornock, R. 2001, *IAU Circ.* # 7644
- Foukal, P., Little, R., & Mooney, J. 1989, *ApJ*, 336, L33
- Froning, C. S., & Robinson, E. L. 2001, *AJ*, 121, 2212 (FR)
- Gelino, D. M., Harrison, T. E., & McNamara, B. J. 2001, *AJ*, 122, in press (Paper 1; astro-ph #0105064)
- Gray, D. F. 1992, *Cambridge Astrophysics Series #20, The Observations and Analysis of Stellar Photospheres* (New York: Cambridge University Press)

- Greiner, J., et al. 2001, *Nature*, submitted
- Haswell, C. A., Robinson, E. L., Horne, K., Stiening, R. F., & Abbott, T. M. C. 1993, *ApJ*, 411, 802 (HRHSA)
- Hauschildt, P. H., Allard, F., & Baron, E. 1999a, *ApJ*, 512, 377
- Hauschildt, P. H., Allard, F., Ferguson, J., Baron, E., & Alexander, D. R. 1999b, *ApJ*, 525, 871
- Hoard, D. W., & Szkody, P. 1996, *ApJ*, 470, 1052
- Iben, I., Tutukov, A. V., & Fedorova, A. V. 1997, *ApJ*, 486, 955
- Johnson, H. L. 1966, *AR A&A*, 4, 193
- Khruzina, T. S. & Cherepashchuk, A. M. 1995, *Astr. Rep.*, Vol 39, #2, 178
- King, N. L., Harrison, T. E., & McNamara, B. J. 1996, *AJ*, 111, 1675
- Leggett, S. K., Allard, F., Geballe, T. R., Hauschildt, P. H., Schweitzer, A. 2001, *ApJ*, 548, 908
- Leibowitz, E. M., Hemar, S., & Orio, M. 1998, *MNRAS*, 300, 463
- Marsh, T. R., Robinson, E. L., & Wood, J. H. 1994, *MNRAS*, 266, 137 (MRW)
- McClintock, J. E., & Remillard, R. A. 1986, *ApJ*, 308, 110
- McClintock, J. E., & Remillard, R. A. 1990, *ApJ*, 350, 386
- McClintock, J. E., Horne, K., & Remillard, R. A. 1995, *ApJ*, 442, 358
- McClintock, J. E., & Remillard, R. A. 2000, *ApJ*, 531, 956
- McClintock, J. E., Garcia, M. R., Caldwell, N., Falco, E. E., Garnavich, P. M., & Zhao, P. 2001, *ApJ*, 551, L147
- Mikami, T., & Heck, A. 1982, *PASJ*, 34, 529
- Murdin, P., Allen, D. A., Morton, D. C., Whalen, J. A. J., & Thomas, R. M. 1980, *MNRAS*, 192, 709
- Nordlund, Å., & Vaz, L.P.R. 1990, *A&A*, 228, 231
- Oke, J.B. 1977, *ApJ*, 217, 182
- Orosz, J. A., Bilyn, C. D., Remillard, R. A., McClintock, J. E., & Foltz, C. B. 1994, *ApJ*, 436, 848
- Orosz, J. A., & Hauschildt, P. H. 2000, *A&A*, 364, 265

- Orosz, J. A., van der Klis, M., McClintock, J. E., Jain, R. K., Bailyn, C. D., & Remillard, R. A. 2001, ATEL #70
- Press, W. H., Teukolsky, S. A., Vetterling, W. T., & Flannery, B. P. 1992, Numerical Recipes in FORTRAN: The Art of Scientific Computing, 2nd edn., (Cambridge: Cambridge University Press)
- Seaton, M. J. 1979, MNRAS, 187, 73P
- Shahbaz, T., Bandyopadhyay, R. M., & Charles, P. A. 1999, A&A, 346, 82
- Shahbaz, T., Naylor, T., & Charles, P. A. 1994, MNRAS, 268, 756 (SNC)
- Shahbaz, T., Naylor, T., & Charles, P. A. 1997, MNRAS, 285, 607
- Vogt, S. S. 1975, ApJ, 199, 418
- Wilson, R.E. 1998, in Reference Manual to the Wilson-Devinney Program, Computing Binary Star Observables, Version 1998 (Gainesville, FL: Univ. Florida)
- Wu, C.-C., Aalders, J. W. G., van Duinen, R. J., Kester, D., & Wesselius, P. R. 1976, A&A, 50 445

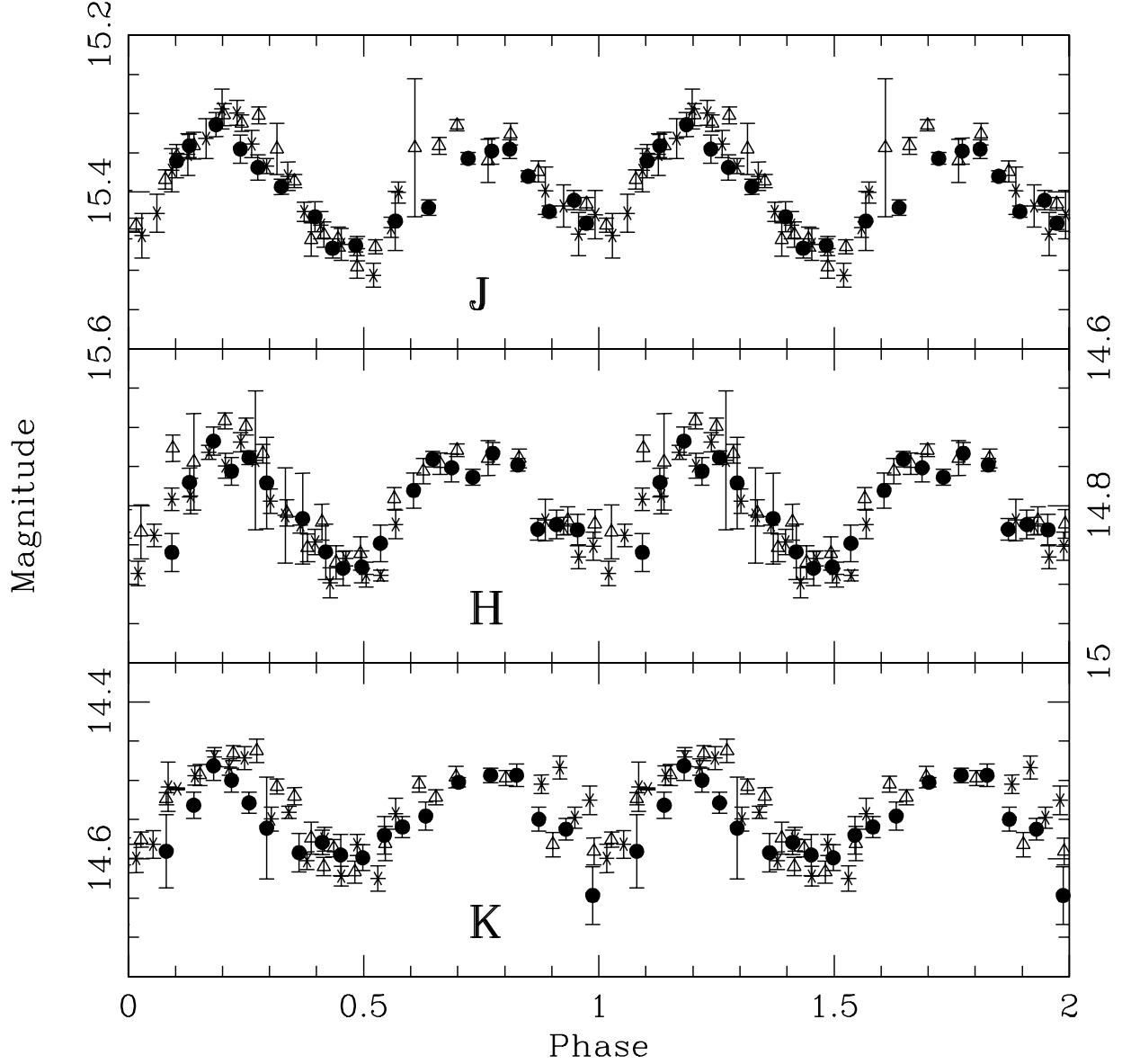


Fig. 1.— SQUID *J*-, *H*-, and *K*- band data taken on 2000 December 8 (filled circles), 9 (open triangles), and 11 (asterisks), with the 2.1 meter telescope at Kitt Peak National Observatory. The data are plotted over two phase cycles for clarity and are phased to the Leibowitz, Hemar, & Orio (1998) ephemeris shifted by 0.5 in phase so that phase 0.0 represents the inferior conjunction of the secondary star. Error bars are  $1\sigma$ . There are no significant night-to-night variations.

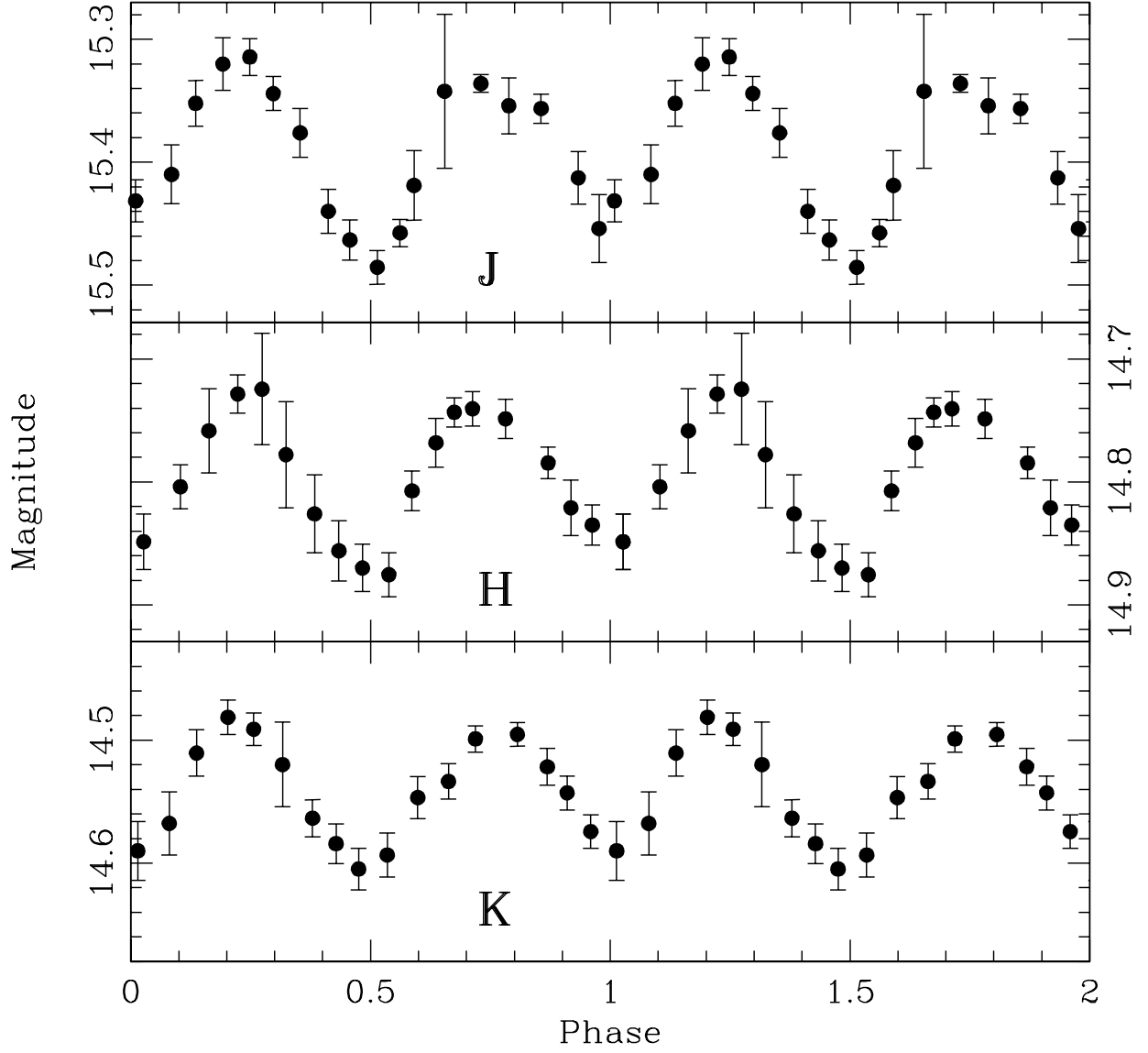


Fig. 2.— Final 2000 December V616 Mon  $J$ -,  $H$ -, and  $K$ - band light curves. Here, the data from Figure 1 were binned in phase in order to obtain one light curve per band. Error bars are  $1\text{-}\sigma$ .

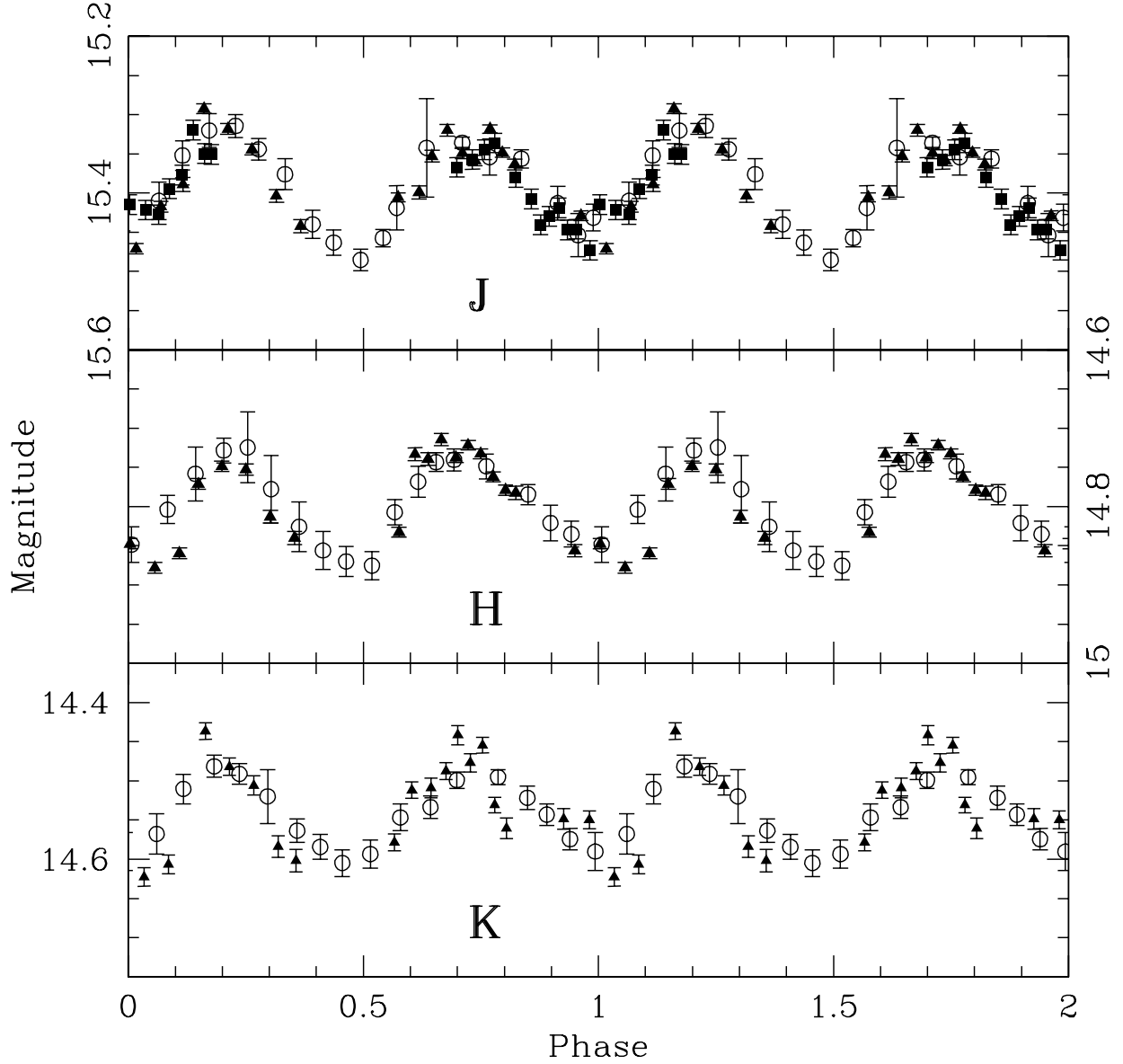


Fig. 3.— Long-term infrared light curves of V616 Mon. The  $J$ - band data span 22.5 months while the  $H$ - and  $K$ - band data span 10.5 months. The open circles represent the SQUID data taken on 2000 December 8, 9, and 11 as plotted in Figure 2. The filled triangles represent the data taken with IRIM at the 2.1 m telescope at Kitt Peak National Observatory on 2000 February 12 and 16. The filled squares in the  $J$ - band light curve represent data taken using GRIM II on the Astrophysical Research Consortium 3.5 m telescope at Apache Point Observatory on 1999 February 25. There are no obvious long-term variations in the shapes or mean magnitudes of the light curves.

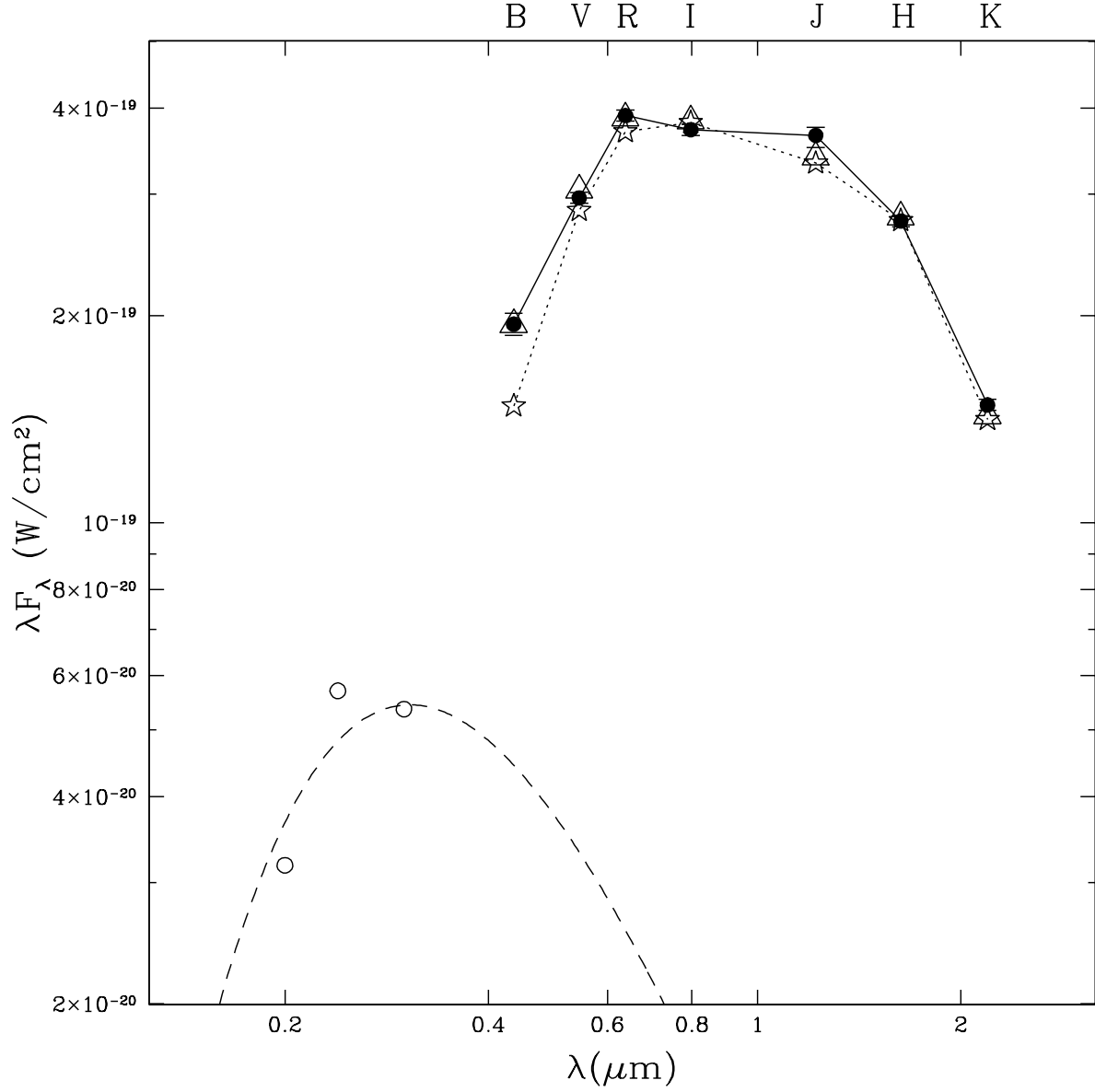


Fig. 4.— The 2000/2001 V616 Mon optical/infrared spectral energy distribution (SED) dereddened by  $A_V = 1.21$  magnitudes (filled circles), compared to the SED of a K4V (open stars) normalized at  $H$ . The two SEDs match well within the errors with small exceptions at  $B$  and  $J$ . The dashed line is a 12000 K blackbody representing the hot spot on the accretion disk. This blackbody is consistent with the dereddened ultraviolet observations taken by McClintock & Remillard (2000) (open circles), and when added to the SED of the K4V (open triangles), explains the observed excess at  $B$ , and provides an excellent fit at the other wavelengths.



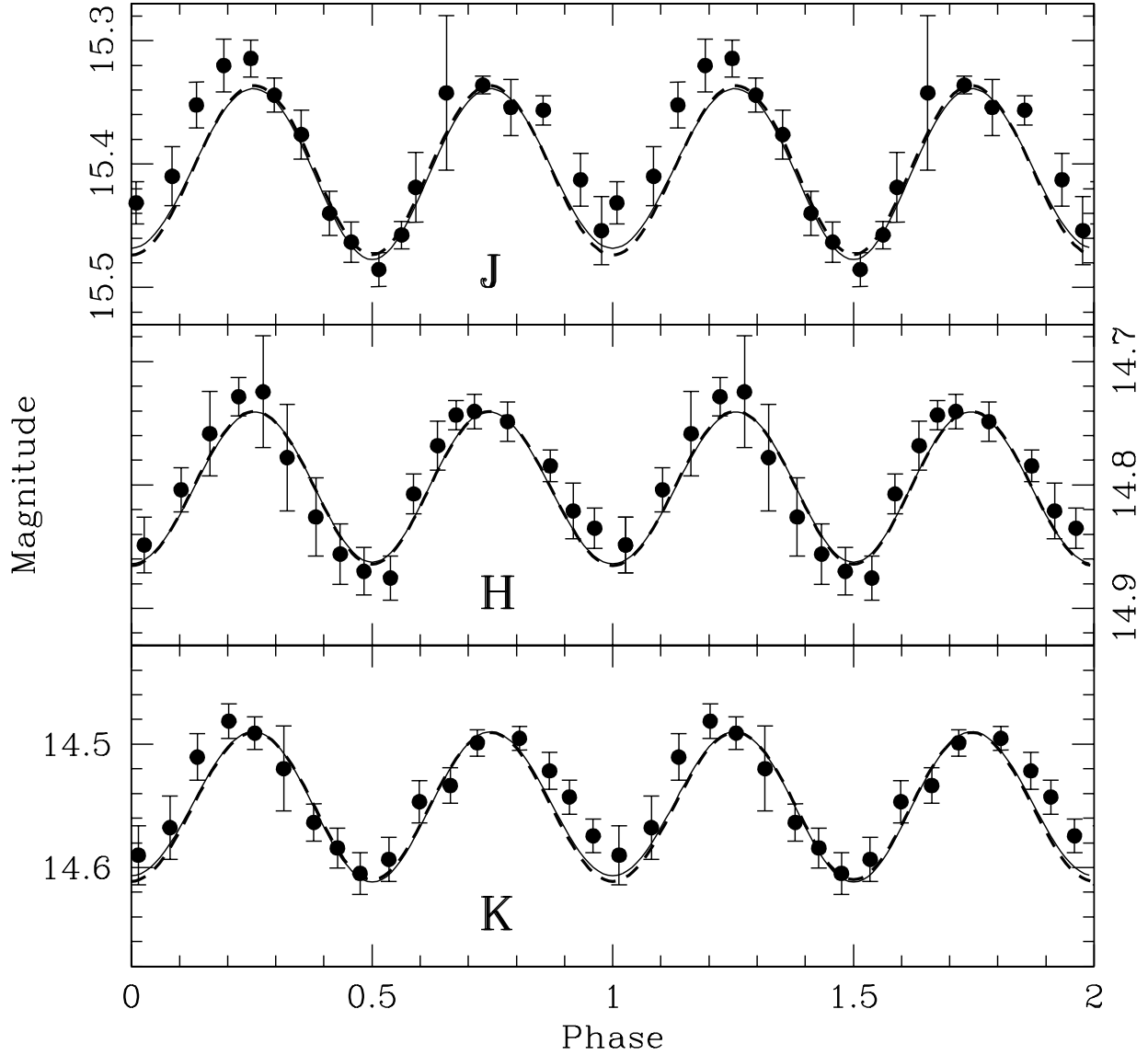


Fig. 5.— The data from Figure 2 (points) and the best fitting models for a K4V secondary star. The WD98 model (solid line) was determined from  $\chi^2$  tests and has  $i = 40^\circ$ . The ELC model (dashed line) was found using its grid search program, and also has  $i = 40^\circ$ . These simple ellipsoidal models are nearly indistinguishable. A small excess is present in the rise to the first maximum, while the second minimum is more shallow than either model.

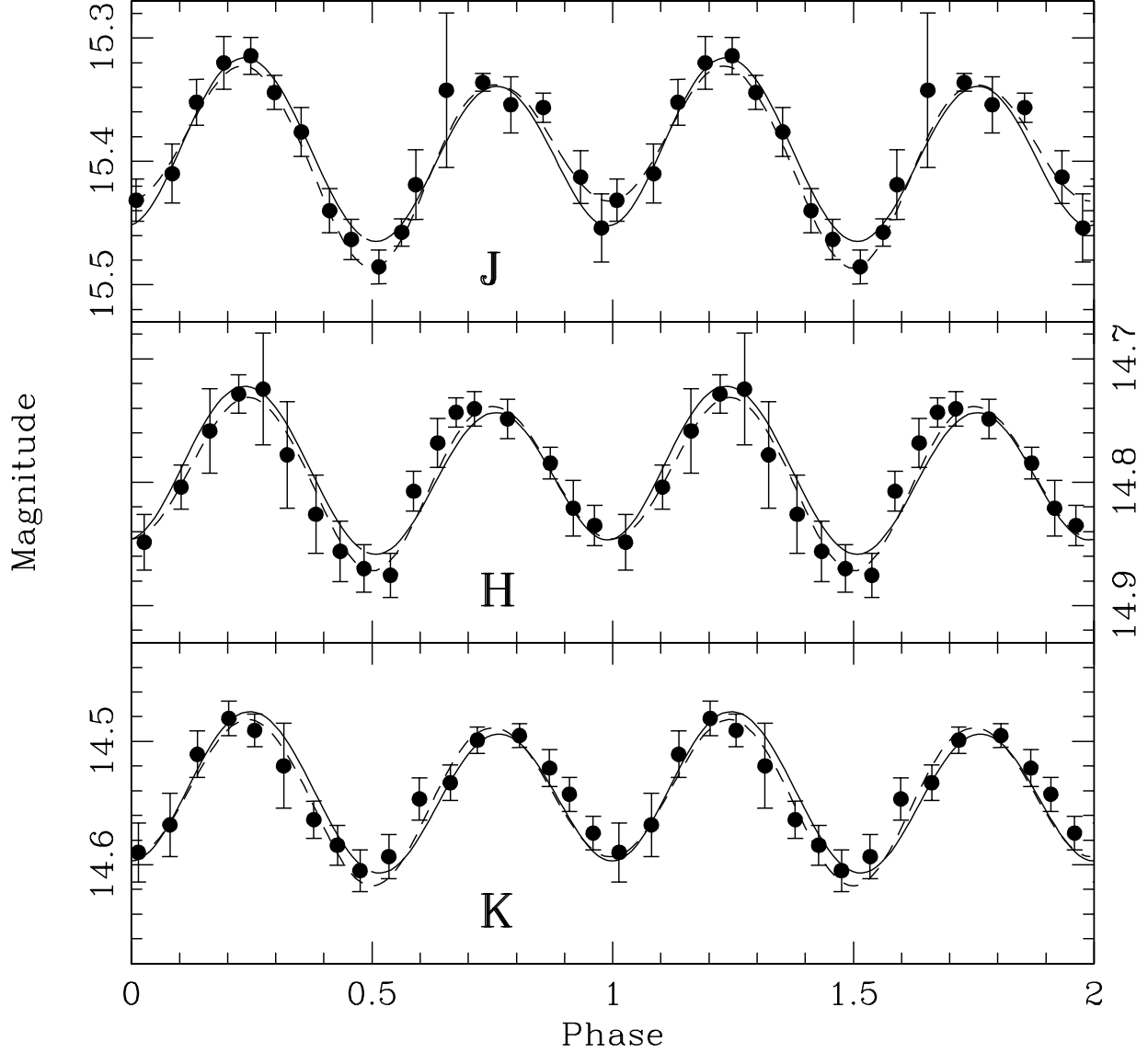


Fig. 6.— The data from Figure 2 (points) and the best fitting cool spot models. The solid line is the WD98 model ( $i = 40^\circ$ ) with a 3600 K spot centered on the equator and at a longitude of  $135^\circ$  with a radius of  $18^\circ$  (4% coverage). The dashed line is the ELC model ( $i = 41^\circ$ ) with a 3495 K spot centered at a latitude of  $172^\circ$  and a longitude of  $0^\circ$  with a radius of  $87^\circ$  (93% coverage). The hot spot models had similar fits, however, they could not be easily explained.

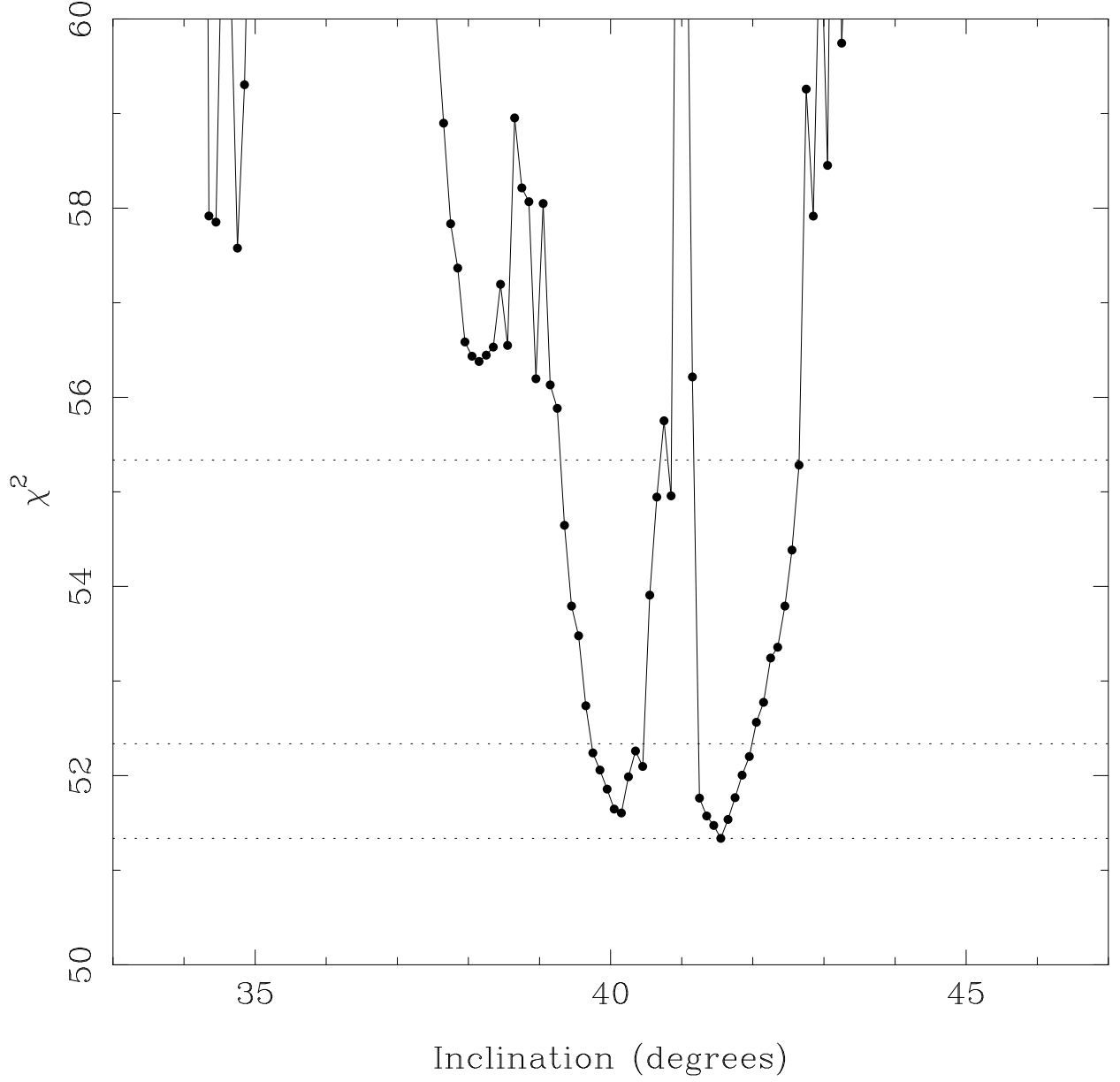


Fig. 7.— The “lower envelope” of the  $\chi^2$  values as a function of the inclination found by the ELC genetic fitting routine for the spotted secondary star models (with no disk). The dotted lined denote the minimum  $\chi^2$  value  $\chi^2_{\min}$ ,  $\chi^2_{\min} + 1$ , and  $\chi^2_{\min} + 4$ .

Table 1. Quiescent Infrared and Optical Colors of V616 Mon

| Reference                 | V          | B - V     | V - R     | V - I     | J          | J - H     | J - K     | Year <sup>a</sup> |
|---------------------------|------------|-----------|-----------|-----------|------------|-----------|-----------|-------------------|
| 1                         | 18.35      | 1.35      | ...       | ...       | ...        | ...       | ...       | 1976              |
| 2                         | 18.2±0.1   | ...       | ...       | ...       | ...        | ...       | ...       | 1978              |
| 3                         | 18.22±0.03 | 1.25      | 1.08      | ...       | ...        | ...       | ...       | 1986/1987         |
| 4                         | ...        | ...       | ...       | ...       | 15.44±0.01 | ...       | 0.89      | 1990              |
| 5                         | 18.20±0.05 | ...       | ...       | ...       | ...        | ...       | ...       | 1992              |
| 5                         | 18.25±0.08 | ...       | ...       | ...       | ...        | ...       | ...       | 1995/1996         |
| 6                         | ...        | ...       | ...       | ...       | 15.6±0.1   | 0.76      | ...       | 1996              |
| 5                         | 18.37±0.05 | ...       | ...       | ...       | ...        | ...       | ...       | 1998              |
| 7                         | 18.27±0.04 | 1.21±0.04 | 0.83±0.04 | 1.57±0.04 | 15.40±0.04 | 0.60±0.04 | 0.85±0.04 | 2000/2001         |
| K4V ( $A_V = 1.21$ mag)   |            | 1.46      | 0.82      | 1.65      |            | 0.70      | 0.88      |                   |
| K4III ( $A_V = 1.21$ mag) |            | 1.80      | 0.93      | 1.99      |            | 0.86      | 1.08      |                   |

<sup>a</sup>Year the data were taken

References. — (1) Oke 1977; (2) Murdin et al. (1980); (3) HRHSA; (4) SNC; (5) McClintock & Remillard 2000; (6) FR; (7) This Paper

Table 2. Wavelength Independent WD98 Input Parameters for V616 Mon

| Parameter                                     | Value        |
|---|--------------|
| Orbital Period (days)                         | 0.323016     |
| Ephemeris (HJD phase 0.0) <sup>a</sup>        | 2450000.025  |
| Semi-Major Axis ( $R_\odot$ )                 | 4.6          |
| Orbital Eccentricity                          | 0.0          |
| Temperature of K4V Secondary (K)              | 4600         |
| Mass Ratio ( $M_2/M_1$ )                      | 0.067        |
| Atmosphere Model                              | Kurucz       |
| Limb Darkening Law                            | Square-root  |
| Secondary Star Gravity Darkening Exponent     | $\beta=0.40$ |
| Secondary Star Bolometric Albedo <sup>b</sup> | 0.676        |

<sup>a</sup>From Leibowitz, Hemar, & Orio (1998); Corresponds to phase 0.0 for light curves presented in this paper, and phase 0.5 from their paper.

<sup>b</sup>From Nordlund & Vaz (1990)

Table 3. Wavelength Dependent WD98 Input Parameters for V616 Mon

| Secondary Star Parameter                             | J     | H      | K      |
|--|-------|--------|--------|
| Monochromatic Luminosity ( $L_{\odot}$ )             | 0.223 | 0.281  | 0.296  |
| Square-root Limb Darkening Coefficient $x_{\lambda}$ | 0.110 | -0.063 | -0.166 |
| Square-root Limb Darkening Coefficient $y_{\lambda}$ | 0.531 | 0.652  | 0.724  |

Table 4. Derived Parameters for V616 Mon

| Parameter                                   | Value            |
|---|------------------|
| Black Hole Mass $M_1$ ( $M_{\odot}$ )       | $11.0 \pm 1.9$   |
| Secondary Star Mass $M_2$ ( $M_{\odot}$ )   | $0.68 \pm 0.18$  |
| Total Mass ( $M_{\odot}$ )                  | $11.70 \pm 2.05$ |
| Orbital Separation $a$ ( $R_{\odot}$ )      | $4.47 \pm 0.27$  |
| Secondary Star Radius $R_2$ ( $R_{\odot}$ ) | $0.80 \pm 0.07$  |
| Secondary Star Gravity ( $\log g$ cgs)      | $4.46 \pm 0.04$  |
| Absolute Magnitude, $J$                     | $4.77 \pm 0.23$  |
| Absolute Magnitude, $H$                     | $4.17 \pm 0.20$  |
| Absolute Magnitude, $K$                     | $4.11 \pm 0.20$  |
| Distance Modulus, $J$ (mag)                 | $10.29 \pm 0.23$ |
| Distance Modulus, $H$ (mag)                 | $10.40 \pm 0.21$ |
| Distance Modulus, $K$ (mag)                 | $10.30 \pm 0.21$ |
| Adopted Distance (pc)                       | $1164 \pm 114$   |